Microfabricated arrays for high-throughput screening of cellular response to cyclic substrate deformation

Christopher Moraes,[ab] Jan-Hung Chen,[ab] Yu Sun*[ab] and Craig A. Simmons*[abc]

Received 17th July 2009, Accepted 19th October 2009
First published as an Advance Article on the web 16th November 2009
DOI: 10.1039/b914460a

Mechanical forces play an important role in regulating cellular function and have been shown to modulate cellular response to other factors in the cellular microenvironment. Presently, no technique exists to rapidly screen for the effects of a range of uniform mechanical forces on cellular function. In this work, we developed and characterized a novel microfabricated array capable of simultaneously applying cyclic equibiaxial substrate strains ranging in magnitude from 2 to 15% to small populations of adherent cells. The array is versatile, and capable of simultaneously generating a range of substrate strain fields and magnitudes. The design can be extended to combinatorially manipulate other mechanobiological culture parameters in the cellular microenvironment. As a first demonstration of this technology, the array was used to determine the effects of equibiaxial mechanical strain on activation of the canonical Wnt/β-catenin signaling pathway in cardiac valve mesenchymal progenitor cells. This high-throughput approach to mechanobiological screening enabled the identification of a novel co-dependence between strain magnitude and duration of stimulation in controlling β-catenin nuclear accumulation. More generally, this versatile platform has broad applicability in the fields of mechanobiology, tissue engineering and pathobiology.

Introduction

The large number of factors in the cellular milieu that can impact biological function has necessitated the development of high-throughput approaches to study cell behavior *in vitro*. Microtechnologies have enabled rapid screening of cellular response to biomaterials,[1] extracellular matrix proteins,[2] cell–cell interactions,[3,4] substrate stiffness,[5] soluble factors[6] and chemical gradients.[7] More recently, the development of multimodal high-throughput stimulation platforms[6,8] has demonstrated interesting combinatorial effects between stimulation types. Such platforms are of particular relevance to research in tissue engineering and drug discovery, as they show that cellular response is dependent on multiple factors in the cellular microenvironment.

Mechanical forces play an important role in driving critical cellular processes, such as apoptosis, matrix deposition, gene and protein expression[9,10] and stem cell differentiation.[11] Mechanical factors have also been shown to modulate cellular response to other stimuli, including matrix proteins,[12] chemical cues,[13] and genetic therapies.[14] In some cases, mechanical factors can supplant other stimuli in driving cellular response.[11] Thus, mechanical cues are important considerations when defining the cellular microenvironment and investigating its effect on cell fate and function. However, despite the demonstrated importance of mechanical forces in regulating and modulating cellular function, high-throughput screening for cellular response is typically conducted in mechanically static conditions.

The *in vivo* mechanical environment is complex and combines a number of loading modalities. Fluid-related stimulation has been successfully recreated on microfabricated platforms, in which microfluidic channels have been used to apply hydrostatic pressures[15] and shear stresses[16,17] to cultured cells. Progress has also been made in developing substrate deformation-based stimulation platforms in which cells are "stretched". The braille display-actuated system developed by Kamotani *et al.*[18] can screen for the effects of stimulation frequency, but is unable to generate uniform strains or probe cellular response to a range of strain magnitudes. Microdevices developed by Tan *et al.*[19] are capable of screening for cellular response to multiple substrate deformations, but a single experiment is limited to three anisotropic biaxial strains at a fixed magnitude, and cells have been shown to differentially respond to distinct strain fields and magnitudes.[20] Furthermore, the system cannot be readily expanded to screen for the integrated cellular response to multiple mechanobiological parameters.

In this paper, we present an array-based microfabricated platform designed to simultaneously apply a range of cyclic uniform substrate strains to single cells or small colonies of cells. In contrast to existing mechanical stimulation systems, the microfabricated array can currently conduct high-throughput screens for the effects of strain magnitude and has been specifically designed to integrate with other microtechnologies that enable individual control over the extracellular matrix, fluid shear stresses, and chemical stimulation applied to isolated cell colonies, thereby enabling massively parallel combinatorial screening for mechanobiological culture parameters.

[a]*Department of Mechanical and Industrial Engineering, University of Toronto, 5 King's College Road, Toronto, Ontario, Canada M5S 3G8. E-mail: simmons@mie.utoronto.ca; sun@mie.utoronto.ca; Fax: +1 416 978 7753; Tel: +1 416 946 0548; +1 416 978 7753; +1 416 946 0549*
[b]*Institute of Biomaterials and Biomedical Engineering, University of Toronto, 164 College Street, Toronto, Ontario, Canada M5S 3G9*
[c]*Faculty of Dentistry, University of Toronto, 124 Edward Street, Toronto, Ontario, Canada M5G 1G6*

As a first demonstration of this technology, the platform was used to probe the temporal and strain magnitude-dependent accumulation of β-catenin in the nuclei of a primary mesenchymal progenitor cell population.[21] β-Catenin is a critical protein in the canonical Wnt signaling pathway that regulates the proliferation and differentiation of mesenchymal progenitor cells.[22–25] In the absence of signals from the canonical Wnt pathway, cytoplasmic levels of β-catenin are maintained through the action of a β-catenin destruction complex. In the presence of Wnt signaling molecules, this destruction complex is inactivated, resulting in hypophosphorylation of β-catenin and subsequent translocation into the cell nucleus.[23] In the nucleus, β-catenin participates in the differential transcriptional regulation of target genes in a dose-dependent manner.[22–25]

Recent studies have shown that mechanical stimuli alone can induce nuclear translocation of β-catenin.[26–28] Capitalizing on the high-throughput capabilities of the developed platform, we demonstrate that levels of nuclear accumulation of β-catenin in mesenchymal progenitor cells are both time-dependent and strain magnitude-dependent. This relationship would have been challenging to observe using conventional low-throughput techniques. Because of the demonstrated link between levels of β-catenin present in the nucleus and stem cell differentiation,[22–25] these results may have implications for processes involving mechanoregulation of cellular differentiation, including tissue engineering, development and the pathobiology of load-bearing tissues.

Experimental methods

Unless otherwise stated, all chemicals and reagents for cell culture were purchased from Sigma-Aldrich (Oakville, ON, Canada); fluorescent dyes from Invitrogen (Burlington, ON, Canada); and all other equipment and materials from Fisher Scientific (Ottawa, ON, Canada).

Device design and simulation

The design of each element within the microdevice array has similarities to the macroscale system described by Schaffer *et al.*[29] Each unit on the microfabricated array (Fig. 1A) consists of a loading post suspended over an actuation cavity. Positive pressure applied to this cavity distends the loading post upwards, which deforms a flexible cell culture substrate (Fig. 1B–E). A lubricant between the loading post and the culture membrane prevents stiction between the two materials. Simultaneous application of a range of substrate strains across the array was achieved by changing the size of the actuation cavity, while keeping the size of the loading posts constant. For a single applied pressure, an increase in actuation cavity size leads to an increase in vertical displacement of the loading post, which in turn creates a higher strain magnitude on the cell culture substrate. Because the loading posts have identical dimensions, the sizes of the mechanically stimulated areas remain constant across the array. Finite element simulations to assess the feasibility of this actuation scheme were conducted in ANSYS (ANSYS Inc., Canonsburg, PA, USA).

Device fabrication

The device consists of multiple layers of patterned poly(dimethylsiloxane) (PDMS, Dow Corning, purchased through A.E. Blake Sales Ltd, Toronto, ON, Canada), fabricated using multilayer soft lithography.[30] To fabricate the three-layer PDMS base structure (Fig. 2), three master molds were fabricated on 3″ × 2″ glass slides, with SU-8 negative photoresist (Microchem, Newton, MA, USA). Sandwich mold fabrication[31] was used to produce three patterned layers of PDMS on transparencies (Grand & Toy, Toronto, ON, Canada), which were transferred sequentially to a rigid glass slide. This fabrication technique prevents shrinkage between device layers,[32] enabling us to realize large, dense arrays of precisely aligned microstructures (Fig. 1F). Connectors were then attached to the air pressure and lubrication channels. Connectors with a large dead-space volume were used to trap air bubbles from the lubricant before injection into the lubrication channels. For experimental simplicity, all subsequent experiments were conducted on a smaller 6 × 5 array.

Following fabrication of the base platform, an 'actuated' fabrication process was used to complete device construction. In

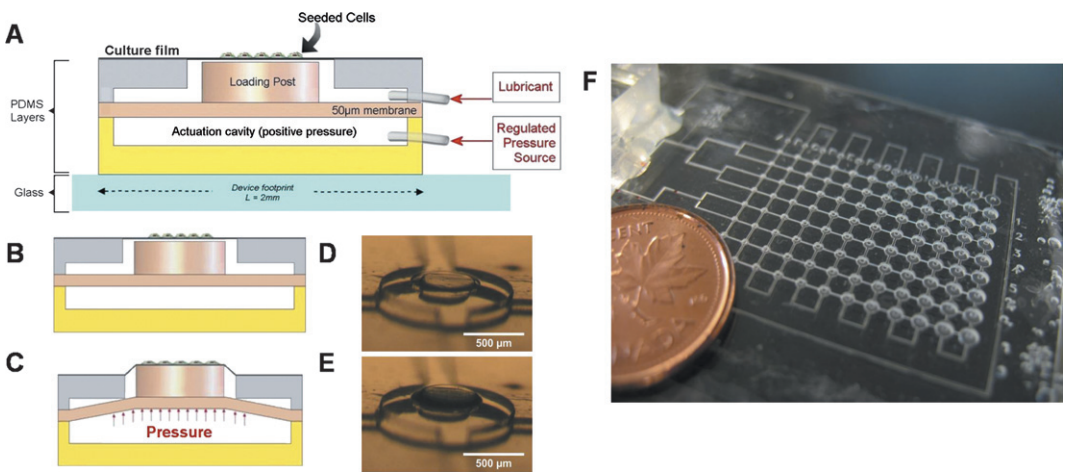

Fig. 1 (A) Schematic cross-sectional view of a single mechanically active unit on the array. (B, C) Schematic of a unit in its (B) resting and (C) actuated positions. (D, E) Stereoscopic images of the device (D) at rest and (E) when actuated. (F) 9 × 12 array of mechanically active culture units, within a 6.5 cm^2 area.

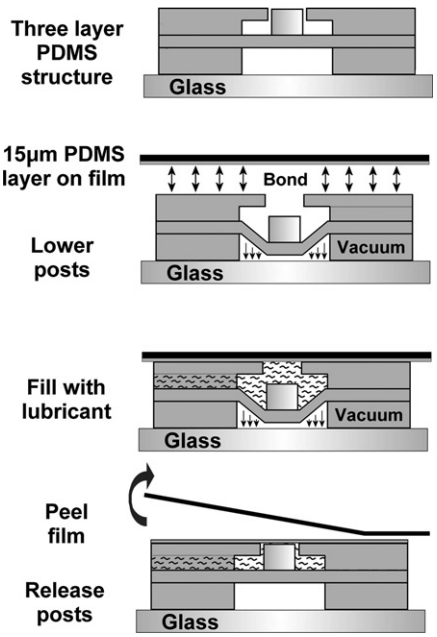

Fig. 2 Fabrication process for mechanically active culture arrays.

these steps (Fig. 2) the device was operated during continued fabrication. A 15 μm thick 'culture film' of PDMS was spin-coated onto a transparency, and cured in an oven for 4 h at 80 °C. A 65 kPa vacuum (Barnant Air Cadet single-head pump) was then applied to the actuation cavities on the base structure, to lower the posts and prevent them adhering to the culture film. The PDMS base structure and culture film surfaces were oxygen plasma treated with a corona discharge unit (Electrotechnic Products, Chicago, IL, USA), placed in contact with each other and heated on a hotplate at 90 °C for 5 min to create a permanent bond.[33] A lubricating solution of 90% glycerol in deionized water was carefully injected into the lubrication channels to fill the spaces between the lowered posts and the culture film. Trapped air pockets were found to shrink over time (as air diffused through the PDMS walls), and it was found that keeping the device at 40 °C removed any trapped air within 10 min. The full procedure was completed within 20 min, which prevented the PDMS surfaces from returning to their hydrophobic states. The loading posts were then released, and the transparency peeled away from the device, leaving the culture film suspended over the lubricated loading posts.

For those devices that were used for cellular studies, a single PDMS gasket was plasma bonded around the device to hold culture media over the cells grown on the array. The devices were then sterilized by soaking in 70% ethanol, air-dried, and exposed to germicidal UV light for 30 min. The device surface was plasma-activated and incubated with 100 μg mL^{-1} Type I collagen (Becton Dickinson, Mississauga, ON, Canada) in 0.02 N acetic acid overnight at 4 °C.

Strain characterization

Characterization of surface strains on the device was conducted by tracking displacements of fluorescent beads. Fluorescent polystyrene beads (Bangs Laboratories, Fishers, IN, USA) of 1 μm in diameter were suspended in methanol and vortexed for 1 min to break up bead aggregates. The bead solution was immediately pipetted onto the device surface, and the methanol was allowed to evaporate. The devices were imaged on a stage heated to 37 °C with a 40× objective (air immersion; 0.6 NA) under a fluorescent microscope (Olympus IX71, Olympus Microscopes, Markham, ON, Canada) when strained and when at rest. Actuation pressures (30 kPa) were applied to the actuation cavities using an eccentric diaphragm pump (SP 500 EC-LC, Schwarzer Precision, Germany).

Bead positions were analyzed using a semi-automated customized algorithm in ImageJ (NIH). Briefly, the images were converted to binary images, and bead locations were tracked between image sets using a modified particle tracking algorithm. A visual representation of particles and displacement vectors was used to manually identify false traces, which were removed from the dataset. The displacement vector sets were then analyzed using a custom-written Matlab code (Mathworks, Natick, MA, USA), to best fit a point from which radial bead displacement originated. This central point was used to calculate changes in radial bead location and an arbitrary reference line was used to calculate changes in circumferential bead location, from which radial and circumferential strain parameters were extracted for each bead. Standard plane fitting algorithms were then used to calculate nominal strain values for each unit in the array. In order to characterize the strains created across a device array, this procedure was repeated for at least three units of each geometry across the array. Graphical results for radial and circumferential strains are reported as mean ± standard error ($n \geq 3$). This procedure was repeated for a second array, with similar results.

To determine the effects of material fatigue on the culture film, the device was placed in cell culture conditions (37 °C, 5% CO_2), and cyclic pressure was applied using a solenoid valve (Pneumadyne, Plymouth, MN, USA), driven at 1 Hz for 10^3, 10^4 and 10^5 cycles. At each of these time points, the strain fields for 15 randomly selected units were characterized using the above-mentioned procedure. Radial strains at each time point were normalized to their initial values, and the results reported as percentage mean ± standard deviation.

Cell culture and immunostaining

Primary porcine aortic valvular interstitial cells (PAVICs) were isolated by enzymatic digestion as previously described[34] and used between passages two and three for all experiments. PAVICs contain a large population of mesenchymal progenitor cells with multilineage differentiation potential, similar to that of mesenchymal stem cells.[21]

Collagen-coated devices were washed three times with phosphate-buffered saline and preconditioned for 2 h at 37 °C with Dulbecco's modified eagle medium (DMEM) supplemented with 10% fetal bovine serum. PAVICs were then seeded on the device surface at 20 000 cells cm^{-2} and maintained in supplemented DMEM for 24 h (37 °C, 5% CO_2) to allow cell spreading and surface attachment. The cell culture arrays were then cyclically stimulated at 1 Hz for 3 and 6 h before fixing the cells in 10% neutral buffered formalin (NBF) overnight at 4 °C.

To detect β-catenin expression, a standard immunocytochemistry procedure was followed. Briefly, NBF-fixed cells were

permeabilized and blocked with 3% bovine serum albumin (BSA). Cells were then incubated with rabbit polyclonal β-catenin antibody (Abcam) followed by AlexaFluor 568 goat anti-rabbit IgG. The cell nuclei were counterstained with Hoechst 33258. Since the devices were maintained in a humidified incubator, condensation of droplets beneath the loading post can hamper imaging using a standard fluorescent microscope. In order to obtain clear images, actuation cavities and the channel network were backfilled with water in a vacuum chamber prior to imaging. Images were then collected using a 40× objective (air immersion, 0.6 NA) on a fluorescent microscope (Olympus IX71, Olympus Microscopes, Markham, ON, Canada) with a CCD camera (QImaging Retiga 2000R, QImaging, Surrey, BC, Canada).

Cell image analysis

Nuclear β-catenin levels were measured by applying a threshold binary function to the nuclear images and manually counting the number of cells in each field of view. The binary images were used to mask the cytoplasmic β-catenin images, and the integrated fluorescent density across all the nuclei was determined. The average β-catenin levels per nucleus were calculated for each image. Nuclear β-catenin levels measured by fluorescent analysis have been shown to correlate directly with those measured by western blotting.[26] Similarly, cytoplasmic β-catenin levels were measured by subtracting the integrated nuclear fluorescent intensity from the integrated cellular fluorescent intensity. The results were reported as mean ± standard deviation ($n = 3$). Data were analyzed using one-way ANOVA tests for each time point. *Post-hoc* pairwise comparisons were conducted using the Student–Newman–Keuls method. All statistical analyses were performed using SigmaStat 3.5 (Systat Software Inc., San Jose, CA, USA).

Results

Computational simulations

Finite element simulations were conducted to test the actuation principle of the device and to determine expected strain field profiles. As a first demonstration of these experiments, circular loading post geometries were used, which theoretically should provide strains equal in magnitude in the radial and circumferential directions (equibiaxial) along the culture film surface.[35] Radial and circumferential strains obtained in the culture region over the 400 μm diameter loading posts (Fig. 3) demonstrated increasing strains with an increase in actuation cavity size, for a single applied pressure of 2.5 kPa. Within a 200 μm diameter region, radial and circumferential strains were relatively uniform, varying by a maximum of 0.22% across this area of interest. The strain field was also isotropic and equibiaxial, with no more than a 0.17% difference between radial and circumferential strains. It was also found that the area of uniform strain decreased with an increase in membrane thickness (data not shown). Consequently, the microdevices were realized with a 15 μm thick culture film, which should significantly improve strain uniformity as compared to the simulation results, which assumed a 20 μm thick film.

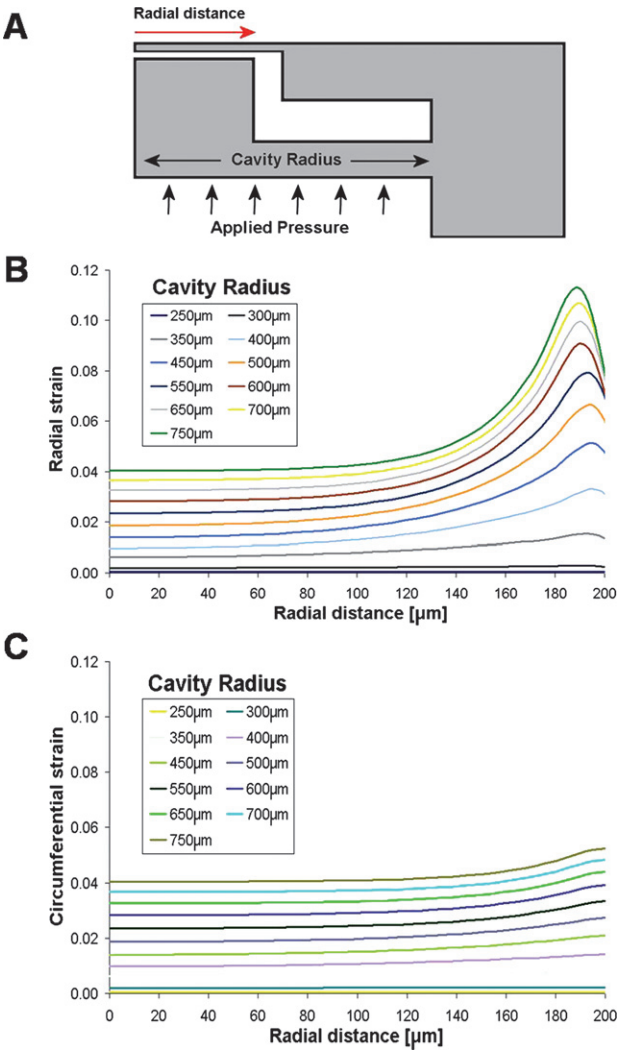

Fig. 3 Finite element simulations demonstrating strain field profiles and device feasibility. (A) Axisymmetric finite element geometry used to obtain a range of (B) radial and (C) circumferential strains across the culture film using a single applied pressure for a range of increasing actuation cavity sizes. Increasing strains are found for increasing sizes of actuation cavity geometry. A uniformity of 0.0022 is obtained within a 100 μm diameter radius, and equality between radial and circumferential strains is within 0.0017.

Device characterization

A typical plot of radial and circumferential strains for a unit on the array is shown in Fig. 4B, with an accompanying line of best fit from linear regression. Measurements of radial strain were found to show a slightly larger spread closer to the center of the loading post, due to limitations in measurement resolution for small bead displacements. Use of this technique to measure circumferential strains was found to be less robust, especially close to the arbitrary reference line. This is due to the measurement resolution limitation and heightened sensitivity of measured circumferential strains to the location of the center of the loading post (the origin of radial deformation), which cannot be precisely determined. However, the ensemble measurement is reasonably accurate and repeatable when using a large number of tracking beads.

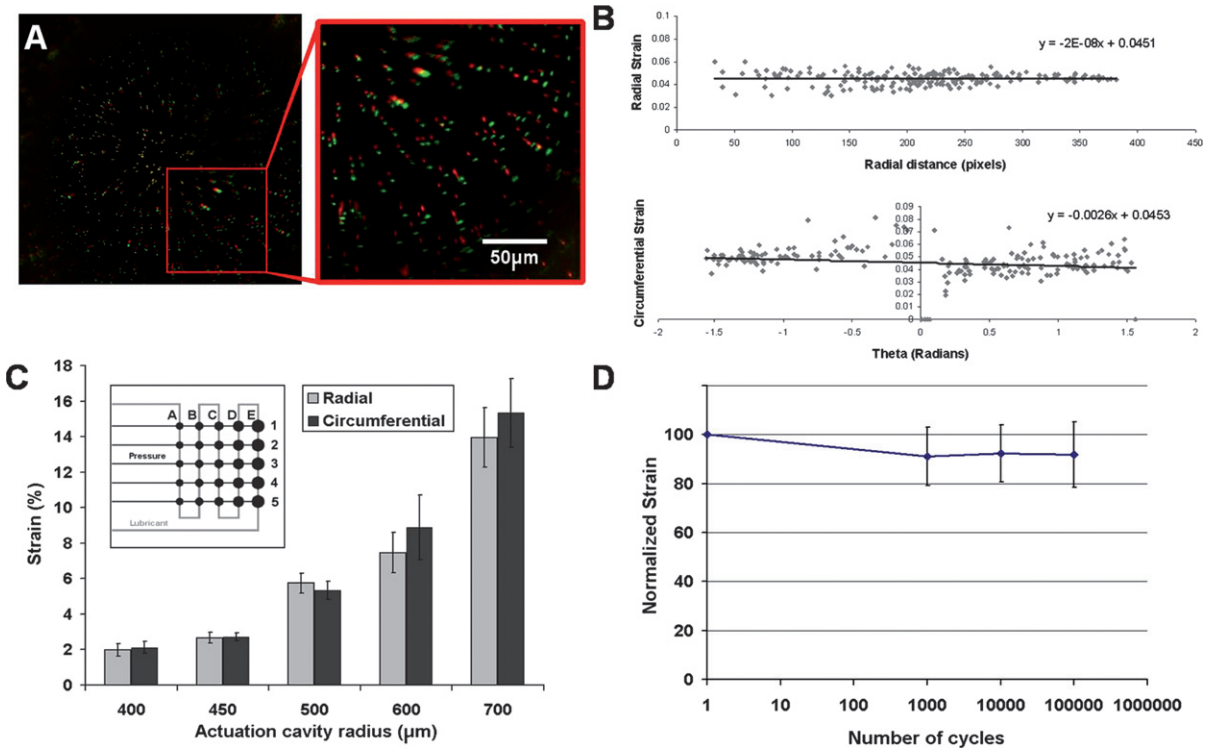

Fig. 4 Characterization of strains on device surface. (A) Fluorescent bead displacement for a single unit on the array, upon device actuation (red: original bead location; green: deformed bead location). (B) Radial and circumferential strains across a single unit on the array, plotted as a function of radial distance and angle from an arbitrary reference line. (C) Radial and circumferential strains (mean ± standard error, $n > 3$) achieved across a 5 × 5 array (inset). (D) Strain values normalized to their initial values after cyclic deformation (mean ± standard deviation, $n = 15$).

A single strain value at the center of each loading post was calculated based on these regression results, in order to compare strain magnitudes across an array actuated at 30 kPa (Fig. 4C). The results demonstrate that the array functioned as intended, providing relatively equal radial and circumferential strains, which increase in magnitude across the array. To simplify data presentation, each actuation cavity size was assigned a nominal strain value based on these results: 2, 3, 5, 8 and 15% for cavity sizes ranging from 800 to 1400 μm in diameter. These strains are within the range of those most often used in macroscale mechanobiological experiments.[10]

Long-term testing of the device was found not to significantly impact the strains produced (Fig. 4D) on any of the units in the array. There were no significant differences in substrate strains after the device operated for 1000, 10 000 or 100 000 cycles ($p = 0.967$). These results demonstrating insignificant levels of material fatigue are supported by long-term fatigue studies of PDMS valves, which have a similar structure and were tested for over four million cycles.[30]

Mechanosensitivity of β-catenin

Levels of cytoplasmic β-catenin were not significantly impacted by stimulation time or strain magnitude (data not shown). However, accumulation of β-catenin in the nuclei of the valve mesenchymal progenitor cells was found to be significantly affected by strain levels and stimulation time (Fig. 5). After 3 h of stimulation, there was a general increase in nuclear β-catenin with increasing strain levels. There was significantly greater β-catenin translocation in cells stimulated at 15% strain than in mechanically static controls ($p = 0.063$). After 6 h of stimulation, there was elevated nuclear β-catenin accumulation in cells stimulated at 3% ($p = 0.093$), 5% ($p = 0.074$), and 8% ($p = 0.005$) strain. However, in cells strained at 15% for 6 h, nuclear β-catenin returned to levels comparable to static controls ($p = 0.827$).

Discussion

High-throughput approaches to studying biological systems have significantly increased the ability to better understand and manipulate cells for tissue engineering, drug discovery and fundamental cell biology studies. Though mechanically active environments have been shown to significantly impact cellular response to other stimuli, most high-throughput screening techniques are limited to mechanically static environments. To address this issue, we have developed a microfabricated platform that can rapidly screen for the effects of multiple cyclic substrate strains. More broadly, the platform can be used in combination with currently available high-throughput screening techniques for other factors that impact cellular function, enabling a massively parallel approach to screening for combinatorial mechanobiological factors in the cellular microenvironment.

The selected device design is versatile in terms of the strain fields that can be applied to individual cell populations. The strain profile on each array unit is dependent on the shape of the loading post.[36] Modifying a single mask in the fabrication process can produce an array with many loading post shapes. Rectangular

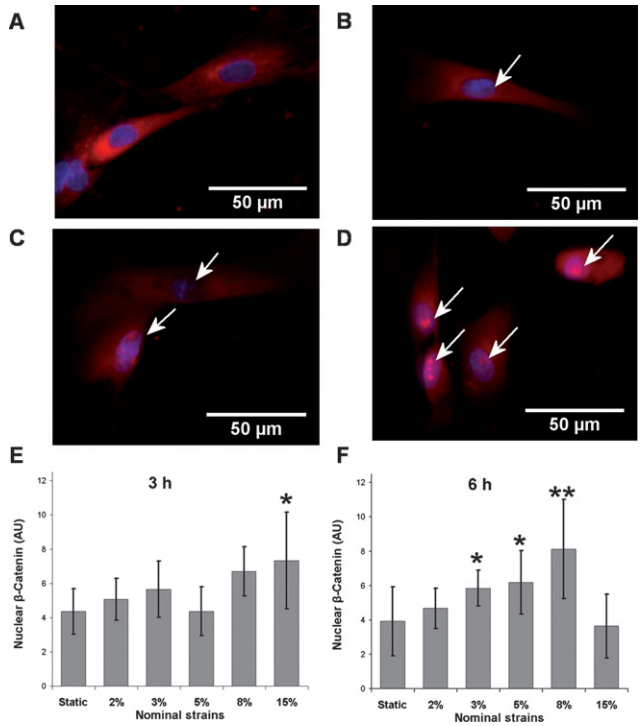

Fig. 5 The influence of mechanical substrate strain on β-catenin accumulation in the nucleus. Representative fluorescent images of cells cultured in (A) static conditions and when subjected to cyclic substrate strains of (B) 3%, (C) 8% and (D) 15% after 3 h of stimulation. Nuclear β-catenin accumulation (arrows) increased with applied strain. (E, F) Integrated nuclear fluorescent intensity quantifying total nuclear β-catenin levels (arbitrary units) after (E) 3 h and (F) 6 h of cyclic substrate strain (*$p < 0.10$; **$p < 0.05$ as compared to the mechanically static condition).

and elliptical posts with changing aspect ratios can create a range of anisotropic biaxial strains. In these initial experiments, the system was limited to circular loading posts, which generate uniform equibiaxial strain fields on the culture films. The strain fields produced are similar to those of the FlexCell systems (FlexCell International Corporation, Hillsborough, NC, USA), the *de facto* standard in macroscale cell stretching systems.[37] Though the maximum strains achievable in the Flexcell systems are as high as 25%, the range of strains actually used in the equibiaxial stimulation of cells most often falls between 3 and 10%,[10] which are well within the operating parameters of the designed device. In contrast to existing macro- and microscale mechanical stimulation systems, our device generates multiple uniform strain levels on a single platform and when scaled up can provide a 256-fold increase in experimental throughput over commercially available systems. Thus, the versatility and increased throughput of the microfabricated platform provide advantages that can speed discovery and improve our understanding of mechanoregulation of cell function.

There are three design limitations to the device as presented here. First, the PDMS gasket used to contain the culture media in the present work potentially allows paracrine communication between cell populations across the array. Though the platform has been designed such that the distance between mechanically active units on the array is greater than the diffusion distance of common paracrine signaling molecules,[37] convective transport and mechanical agitation caused by the moving loading posts remain a concern. In order to address this issue, the device was designed to allow cells to be cultured on a large, flat, unobstructed surface. Hence, simple PDMS wells can be integrated on the flat culture surface of the device to segregate soluble paracrine cues on different portions of the array. The pitch between elements in the array was designed based on the standard 1536-well plate format to allow commercial robotic liquid handling equipment to automatically control chemical stimulation factors across such an array of wells. Alternatively, microfluidic networks can also be used to control chemical stimulation or apply shear stresses to specific areas of the array. Hence, this platform design can be extended to enable screening for the effects of combinations of mechanical and chemical cues.

Second, a common problem associated with loading post-based deformation systems is that cells experience heterogeneous strains away from the center of the loading post. The ability to spatially control cellular adhesion patterns across the array can address this issue. The flat device surface allows adhesive extracellular matrix proteins to be readily printed on the surface using well-established techniques, such as a commercially available protein plotters,[2] a PDMS stamp for microcontact printing,[38] or an elastomeric stencil to apply matrix protein solutions to specific areas of the device.[39] Furthermore, such an approach would extend the capabilities of the system to manipulate extracellular matrix protein type and concentrations in combination with cyclic mechanical substrate strain.

Third, this platform is not well-suited to real-time imaging of cells under mechanical stimulus using simple microscopy, as the culture membrane is displaced out of the focal plane. Though this can be achieved using auto-focusing microscopy systems or post-processing image manipulation algorithms, these are non-trivial solutions. Furthermore, the primary advantage to this research platform is in experimental throughput; assessing real-time cellular response to multiple mechanical stimuli would require simultaneous imaging of all the units in the array, which would require complex imaging systems. Hence, the system has been designed for and is best suited to determine end-point biological response to a range of mechanical substrate strain conditions.

Moving to a microfabricated format when designing mechanically active culture systems yields a number of generic advantages: smaller quantities of expensive cell culture and immunostaining reagents are used; the experimental equipment has a significantly reduced footprint; a single fabrication step can be used to generate a large number of experimental conditions without manual intervention; the length scale is ideally suited for single cell studies; cells can be visualized directly on-chip using bright field or fluorescent microscopy; and the potential for completely automated experimental techniques can be more easily realized. Additionally, unlike macroscale systems,[40] applied strain levels in the microscale system did not change at high cycle numbers. Furthermore, microfabrication of mechanically active cell culture platforms also brings a specific advantage that is not possible on similar macroscale instruments. Mechanically straining cells on deforming substrates generates reactive normal fluid stresses caused by dragging the cells through the culture media, which can unintentionally influence cell function.[41] Because cells must be cultured under liquid

media, these two forms of mechanical stimulation cannot be decoupled. On the microscale, however, the total perturbation to the system required to produce a specific strain is significantly reduced. For example, creating a 15% substrate strain in a 3.6 cm diameter well plate requires the substrate to be stretched by 540 mm. Creating a similar substrate strain in a 500 μm diameter film requires the substrate to be stretched by 75 μm, reducing the distance through which cells are displaced by nearly 4 orders of magnitude. Though the issue of unintentional loading stresses is not completely eliminated, this platform reduces reactive normal forces and their confounding effects on the response of cells to substrate stretch.

Designing mechanically active culture experiments on the microscale also has limitations, specifically: (1) reduction in numbers of cells; (2) increase in stiction forces; and (3) material limitations of microfabrication. First, because of the reduced number of cells available for analyses, the utility of the mechanically active array is limited to high-level screens for fluorescently tagged proteins or morphological assays. The reduction in the number of mechanically stimulated cells makes techniques such as RT-PCR, ELISA and western blotting challenging with current technologies. Hence, as is the case with most high-throughput screening systems, this array is best suited for narrowing research focus to certain specific microenvironmental parameters of interest.

Reducing the size of system components increases the problem of stiction between the loading post and the cell culture film. In this microdevice, solid PDMS microstructures are required to interact with a low coefficient of friction. Hence, selection of an appropriate lubricant was critical for successful device operation. Standard lubricants and oils were unsuitable because they migrated through the PDMS, caused swelling, and in some cases were toxic to cultured cells. Glycerol is biocompatible, does not swell PDMS,[42] and has been shown to have a low coefficient of friction between hydrophilic PDMS surfaces.[43] Because oxygen plasma-activated PDMS surfaces maintain their hydrophilic nature under water,[44] the fabrication process was designed to rapidly cover both contact surfaces with a glycerol–water lubricant, shortly after plasma treatment. In this way, the culture film can slip over the post and deform reliably. Experimental characterization showed little difference in generated strain fields when using 30% or 90% glycerol (data not shown), in spite of significant differences in viscosity of the fluids. The fluid viscosity could affect the deformation rate, but has little influence on end-point strains. Visual observations confirmed that maximum deformation was reached well within the applied pressure cycle of 0.5 s when using a 90% glycerol lubricant.

Microfabrication also limits the materials that can be used as a cell culture substrate on these devices. Substrate material has been shown to significantly impact cellular function,[45,46] and though PDMS provides a convenient culture substrate for short term studies such as those reported here, it does not support long-term culture[47] and is not a common biomaterial. Either modifying the PDMS[48] or incorporating alternative biomaterials into the microfabrication process[47] would enable longer-term experiments and potentially improve the translatability of these devices to screen biomaterials for tissue engineering applications.

As an initial demonstration of this technology, the effects of mechanical strain on β-catenin nuclear accumulation were studied in primary mesenchymal progenitor cells derived from the aortic valve interstitium. The aortic valve contains a strikingly large subpopulation of mesenchymal progenitors,[21] which are under constant mechanical strain *in vivo*.[49] Wnt signaling pathway components, including β-catenin, are elevated in valvular interstitial cells in diseased aortic valves,[50] with calcified lesions often occurring in regions subjected to high mechanical stress.[51] Hence, an understanding of how mechanical strain modulates β-catenin nuclear accumulation in valve-derived mesenchymal progenitors may help in understanding the pathobiological basis of aortic valve sclerosis. β-Catenin plays a critical role in regulating mesenchymal progenitor cell proliferation and differentiation and is normally kept at a relatively low level in the cytoplasm by active degradation.[22–24] Upon activation of the canonical Wnt signaling pathway, β-catenin degradation is inhibited and β-catenin is translocated into the nucleus, where it can accumulate and regulate gene transcription.[25] Though mechanical stimuli have been shown to induce nuclear translocation of β-catenin,[26–28] the effects of cyclic strain magnitude and duration on β-catenin regulation are not defined. Our results suggest that though cytoplasmic levels of β-catenin are not substantially affected by applied substrate strains, nuclear accumulation of β-catenin is both time- and strain magnitude-dependent, where large strains accelerate the cycle of nuclear translocation and subsequent degradation. Smaller strains require longer times for protein translocation but achieve similar levels of accumulation. These results identify two hypotheses for further study. First, different magnitudes of substrate strains either differentially affect translocation into the nucleus, or differentially affect the degradation or removal of β-catenin from the nucleus. Either possibility results in the accumulation of nuclear β-catenin, which has a demonstrated effect on cellular function. Second, there is a relationship between substrate strain magnitude and the temporal dynamics of β-catenin nuclear accumulation. Taken together, these initial findings suggest a novel time- and strain-dependent mechanotransduction mechanism by which different strain magnitudes may elicit distinct temporal responses in mesenchymal progenitors. As is the case with most high-throughput screening platforms, these results serve to identify a starting point for further quantitative studies detailing the impact of nuclear β-catenin levels and residence time on cellular function. The current experiments, in which only two variables (strain magnitude and duration) were tested, would have been significantly more time consuming if using existing macroscale equipment, demonstrating the need for high-throughput techniques to study cellular response to multiple mechanobiological stimuli.

Conclusions

A microfabricated array was designed and developed to simultaneously test cellular response to a range of cyclic equibiaxial substrate strains. The device generates uniform strains from 2 to 15% across the array, a range most often used in macroscale experiments. As a first demonstration of this technology, the effects of mechanical stimulation on the differential accumulation of β-catenin in the nuclei of mesenchymal progenitor cells were investigated. The experiments revealed a complex relationship between stimulation time, strain

magnitude, and nuclear accumulation of the protein, an effect that may not have been observed without a high-throughput approach to these studies. More generally, this platform can be used to create a variety of strain fields and can be extended to systematically and combinatorially manipulate multiple mechanobiological parameters, including extracellular matrix, chemical cues, and mechanical stimulation, for high-throughput screening research.

Acknowledgements

We would like to thank Wen Li Kelly Chen for expert technical assistance. We acknowledge microfabrication support from the Emerging Communications Technology Institute and the Toronto Microfluidics Foundry. We acknowledge financial support from the Natural Sciences and Engineering Research Council of Canada and Canadian Institutes of Health Research (CHRPJ 323533-06), the Ontario Graduate Scholarship programs to CM, and the Canada Research Chairs in Micro and Nano Engineering Systems to YS, and in Mechanobiology to CAS.

Notes and references

1 D. G. Anderson, D. Putnam, E. B. Lavik, T. A. Mahmood and R. Langer, *Biomaterials*, 2005, **26**, 4892–4897.
2 C. J. Flaim, S. Chien and S. N. Bhatia, *Nat. Methods*, 2005, **2**, 119–125.
3 E. E. Hui and S. N. Bhatia, *Proc. Natl. Acad. Sci. U. S. A.*, 2007, **104**, 5722–5726.
4 A. M. Skelley, O. Kirak, H. Suh, R. Jaenisch and J. Voldman, *Nat. Methods*, 2009, **6**, 147–152.
5 N. Zaari, P. Rajagopalan, S. K. Kim, A. J. Engler and J. Y. Wong, *Adv. Mater.*, 2004, **16**, 2133–2137.
6 R. Gomez-Sjoberg, A. A. Leyrat, D. M. Pirone, C. S. Chen and S. R. Quake, *Anal. Chem.*, 2007, **79**, 8557–8563.
7 T. M. Keenan, C. H. Hsu and A. Folch, *Appl. Phys. Lett.*, 2006, **89**, 114103.
8 C. J. Flaim, D. Teng, S. Chien and S. N. Bhatia, *Stem Cells Dev.*, 2008, **17**, 29–39.
9 C. A. Simmons, S. Matlis, A. J. Thornton, S. Chen, C. Y. Wang and D. J. Mooney, *J. Biomech.*, 2003, **36**, 1087–1096.
10 J. H. Wang and B. P. Thampatty, *Biomech. Model. Mechanobiol.*, 2006, **5**, 1–16.
11 R. McBeath, D. M. Pirone, C. M. Nelson, K. Bhadriraju and C. S. Chen, *Dev. Cell*, 2004, **6**, 483–495.
12 D. A. MacKenna, F. Dolfi, K. Vuori and E. Ruoslahti, *J. Clin. Invest.*, 1998, **101**, 301–310.
13 W. C. Lee, T. M. Maul, D. A. Vorp, J. P. Rubin and K. G. Marra, *Biomech. Model. Mechanobiol.*, 2007, **6**, 265–273.
14 H. J. Kong, J. Liu, K. Riddle, T. Matsumoto, K. Leach and D. J. Mooney, *Nat. Mater.*, 2005, **4**, 460–464.
15 W. Y. Sim, S. W. Park, S. H. Park, B. H. Min, S. R. Park and S. S. Yang, *Lab Chip*, 2007, **7**, 1775–1782.
16 E. W. K. Young, A. R. Wheeler and C. A. Simmons, *Lab Chip*, 2007, **7**, 1759–1766.
17 J. W. Song, W. Gu, N. Futai, K. A. Warner, J. E. Nor and S. Takayama, *Anal. Chem.*, 2005, **77**, 3993–3999.
18 Y. Kamotani, T. Bersano-Begey, N. Kato, Y. C. Tung, D. Huh, J. W. Song and S. Takayama, *Biomaterials*, 2008, **29**, 2646–2655.
19 W. Tan, D. Scott, D. Belchenko, H. J. Qi and L. Xiao, *Biomed. Microdevices*, 2008, **10**, 869–882.
20 J. S. Park, J. S. Chu, C. Cheng, F. Chen, D. Chen and S. Li, *Biotechnol. Bioeng.*, 2004, **88**, 359–368.
21 J. H. Chen, C. Y. Yip, E. D. Sone and C. A. Simmons, *Am. J. Pathol.*, 2009, **174**, 1109–1119.
22 D. Silkstone, H. Hong and B. A. Alman, *Nat. Clin. Pract. Rheumatol.*, 2008, **4**, 413–419.
23 C. Christodoulides, C. Lagathu, J. K. Sethi and A. Vidal-Puig, *Trends Endocrinol. Metab.*, 2009, **20**, 16–24.
24 C. Y. Logan and R. Nusse, *Annu. Rev. Cell Dev. Biol.*, 2004, **20**, 781–810.
25 M. D. Gordon and R. Nusse, *J. Biol. Chem.*, 2006, **281**, 22429–22433.
26 V. J. Armstrong, M. Muzylak, A. Sunters, G. Zaman, L. K. Saxon, J. S. Price and L. E. Lanyon, *J. Biol. Chem.*, 2007, **282**, 20715–20727.
27 J. A. Robinson, M. Chatterjee-Kishore, P. J. Yaworsky, D. M. Cullen, W. Zhao, C. Li, Y. Kharode, L. Sauter, P. Babij, E. L. Brown, A. A. Hill, M. P. Akhter, M. L. Johnson, R. R. Recker, B. S. Komm and F. J. Bex, *J. Biol. Chem.*, 2006, **281**, 31720–31728.
28 E. J. Arnsdorf, P. Tummala and C. R. Jacobs, *PLoS One*, 2009, **4**, e5388.
29 J. L. Schaffer, M. Rizen, G. J. Litalien, A. Benbrahim, J. Megerman, L. C. Gerstenfeld and M. L. Gray, *J. Orthop. Res.*, 1994, **12**, 709–719.
30 M. A. Unger, H. P. Chou, T. Thorsen, A. Scherer and S. R. Quake, *Science*, 2000, **288**, 113–116.
31 B. H. Jo, L. M. Van Lerberghe, K. M. Motsegood and D. J. Beebe, *J. Microelectromech. Syst.*, 2000, **9**, 76–81.
32 C. Moraes, Y. Sun and C. A. Simmons, *J. Micromech. Microeng.*, 2009, **19**, 065015.
33 K. Haubert, T. Drier and D. Beebe, *Lab Chip*, 2006, **6**, 1548–1549.
34 C. Y. Yip, J. H. Chen, R. Zhao and C. A. Simmons, *Arterioscler., Thromb., Vasc. Biol.*, 2009, **29**, 936–942.
35 C. R. Ethier and C. A. Simmons, *Introductory Biomechanics: From Cells to Organisms*, Cambridge University Press, Cambridge, UK, 2007.
36 J. P. Vande Geest, E. S. Di Martino and D. A. Vorp, *J. Biomech.*, 2004, **37**, 1923–1928.
37 T. D. Brown, *J. Biomech.*, 2000, **33**, 3–14.
38 R. S. Kane, S. Takayama, E. Ostuni, D. E. Ingber and G. M. Whitesides, *Biomaterials*, 1999, **20**, 2363–2376.
39 A. Folch, B. H. Jo, O. Hurtado, D. J. Beebe and M. Toner, *J. Biomed. Mater. Res.*, 2000, **52**, 346–353.
40 F. H. Bieler, C. E. Ott, M. S. Thompson, R. Seidel, S. Ahrens, D. R. Epari, U. Wilkening, K. D. Schaser, S. Mundlos and G. N. Duda, *J. Biomech.*, 2009, **42**, 1692–1696.
41 T. D. Brown, M. Bottlang, D. R. Pedersen and A. J. Banes, *Am. J. Med. Sci.*, 1998, **316**, 162–168.
42 J. N. Lee, C. Park and G. M. Whitesides, *Anal. Chem.*, 2003, **75**, 6544–6554.
43 J. H. H. Bongaerts, K. Fourtouni and J. R. Stokes, *Tribol. Int.*, 2007, **40**, 1531–1542.
44 J. R. Anderson, D. T. Chiu, R. J. Jackman, O. Cherniavskaya, J. C. McDonald, H. Wu, S. H. Whitesides and G. M. Whitesides, *Anal. Chem.*, 2000, **72**, 3158–3164.
45 M. E. Furth, A. Atala and M. E. Van Dyke, *Biomaterials*, 2007, **28**, 5068–5073.
46 R. Langer and D. A. Tirrell, *Nature*, 2004, **428**, 487–492.
47 C. Moraes, Y. K. Kagoma, B. M. Beca, R. L. Tonelli-Zasarsky, Y. Sun and C. A. Simmons, *Biomaterials*, 2009, **30**, 5241–5250.
48 B. J. Klenkler, M. Griffith, C. Becerril, J. A. West-Mays and H. Sheardown, *Biomaterials*, 2005, **26**, 7286–7296.
49 H. Y. Huang, J. Liao and M. S. Sacks, *J. Biomech. Eng.*, 2007, **129**, 880–889.
50 F. C. Caira, S. R. Stock, T. G. Gleason, E. C. McGee, J. Huang, R. O. Bonow, T. C. Spelsberg, P. M. McCarthy, S. H. Rahimtoola and N. M. Rajamannan, *J. Am. Coll. Cardiol.*, 2006, **47**, 1707–1712.
51 M. J. Thubrikar, J. Aouad and S. P. Nolan, *Am. J. Cardiol.*, 1986, **58**, 304–308.

